Rare Metal Materials and Engineering
Volume 55, Issue 1, January 2026
Available online at www.rmme.ac.cn

Science Press

Cite this article as: Jian Changhuang, Yang Yang, Wang Chengyong, et al. Effect of Nb Addition on Tensile and Wear Properties of 18Ni300 Mold Steel Fabricated by LPBF[J]. Rare Metal Materials and Engineering, 2026, 55(01): 18-26. DOI: https://doi.org/10.12442/j.issn.1002-185X.20250031.

ARTICLE

Effect of Nb Addition on Tensile and Wear Properties of 18Ni300 Mold Steel Fabricated by LPBF

Jian Changhuang[1,2], Yang Yang[1], Wang Chengyong[1], Yu Bowen[1,2], Niu Liuhui[2], Hu Gaofeng[2], Liu Jianye[2], Huang Zhenghua[2]

[1] State Key Laboratory of High Performance Tools, School of Electromechanical Engineering, Guangdong University of Technology, Guangzhou 510006, China; [2] Guangdong Provincial Engineering and Technology Research Center for Metal 3D Printing, Guangdong Hanbang 3D Tech Co., Ltd, Zhongshan 528427, China

Abstract: Laser powder bed fusion (LPBF) is highly suitable for forming 18Ni300 mold steel, thanks to its excellent capability in manufacturing complex shapes and outstanding capacity for regulating microstructures. It is widely used in fields such as injection molding, die casting, and stamping dies. Adding reinforcing particles into steel is an effective means to improve its performance. Nb/18Ni300 composites were fabricated by LPBF using two kinds of Nb powders with different particle sizes, and their microstructures and properties were studied. The results show that the unmelted Nb particles are uniformly distributed in the 18Ni300 matrix and the grains are refined, which is particularly pronounced with fine Nb particles. In addition, element diffusion occurs between the particles and the matrix. The main phases of the base alloy are α-Fe and a small amount of γ-Fe. With the addition of Nb, part of the α-Fe is transformed into γ-Fe, and unmelted Nb phases appear. The addition of Nb also enhances the hardness and wear resistance of the composites but slightly reduces their tensile properties. After aging treatment, the molten pools and grain boundaries become blurred, grains are further refined, and the interfaces around the particles are thinned. The aging treatment also promotes the formation of reverted austenite. The hardness, ultimate tensile strength, and volumetric wear rate of the base alloy reach 51.9 HRC, 1704 MPa, and 17.8×10^{-6} mm^3/(N·m), respectively. In contrast, the sample added with fine Nb particles has the highest hardness (56.1 HRC), ultimate tensile strength (1892 MPa) and yield strength (1842 MPa), and the volume wear rate of the sample added with coarse Nb particles is reduced by 90% to 1.7×10^{-6} mm^3/(N·m).

Key words: laser powder bed fusion; 18Ni300 mold steel; Nb addition; microstructure; mechanical property

1 Introduction

Laser powder bed fusion (LPBF) occupies an important position in modern advanced manufacturing technologies, due to its unique advantages. It breaks through the limitations of traditional manufacturing methods in terms of design freedom and the fabrication of complex structures, enabling the production of components with fine internal structures, high-precision dimensions, and excellent mechanical properties. In recent years, LPBF has shown broad application prospects across fields such as injection molding, die casting, and stamping dies, thereby providing a robust impetus for promoting technological progress and innovative development in various industries[1–3]. Thus, LPBF has garnered increasing attention from scholars and manufacturers for its enormous potential.

18Ni300 mold steel is a typical maraging steel with outstanding specific strength, fracture toughness, and ductility[4]. It can be further strengthened through the precipitation of intermetallic compounds during aging treatment[5–7]. Mao et al[8] fabricated 18Ni300 steel samples with high densi-

Received date: January 16, 2025
Foundation item: Key-Area Research and Development Program of Guangdong Province (2023B0909020004); Project of Innovation Research Team in Zhongshan (CXTD2023006); Natural Science Foundation of Guangdong Province (2023A1515011573); Zhongshan Social Welfare Science and Technology Research Project (2024B2022)
Corresponding author: Huang Zhenghua, Ph. D., Professor, Guangdong Provincial Engineering and Technology Research Center for Metal 3D Printing, Guangdong Hanbang 3D Tech Co., Ltd, Zhongshan 528427, P. R. China, E-mail: zhhuang@hb3dp.com; Yang Yang, Ph. D., Professor, State Key Laboratory of High Performance Tools, School of Electromechanical Engineering, Guangdong University of Technology, Guangzhou 510006, P. R. China, E-mail: 342913700@qq.com

fication by LPBF, and reported that the ultimate tensile strength of the samples could reach 1245 MPa. Guo et al[9] demonstrated that LPBF-fabricated 18Ni300 samples subjected solely to aging treatment have comparable strength and hardness to conventionally cast samples that undergo both solution and aging treatments. However, the service lifetime of molds made of this steel failed to meet practical requirements in some harsh environments, thereby posing greater challenges to the strength and wear resistance of the mold steel. To effectively enhance the comprehensive mechanical properties of metals, reinforcing particles, such as oxides, intermetallic compounds, nitrides, carbides, and borides, can be added to the metal matrix[5]. Such materials are called particle-reinforced metal matrix composites (PRMMCs), which benefit from the advantages of both reinforcements and matrix materials[3].

More importantly, LPBF has been proven suitable for fabricating PRMMCs[10–12]. Due to the high temperature gradient of the molten pool and surface tension gradient caused by rapid solidification and strong Marangoni effects in the process, the reinforcing particles can be redistributed in the molten pool, and hence the composites with uniformly dispersed reinforcing particles can be obtained. Li et al[4] studied WC/18Ni300 composites with different WC contents, and found that the WC particles were partially dissolved and uniformly distributed in the matrix. They also noted that the mechanical properties of the samples changed to varying degrees with increasing the WC content, and that the addition of an appropriate number of WC particles could improve the comprehensive properties of the composites. Bhowmik et al[13] observed the microstructure of the LPBF-processed TiC/316L composites and found that due to the small melting zone and fast cooling rate, irregular TiC particles were distributed at dislocation cell boundaries, while fine cuboidal TiC particles were uniformly distributed both across the cell boundaries and within the cells. In addition, due to the differences in thermal expansion coefficients and melting points, some elements of the reinforcing particles and the matrix display significant diffusion behavior during the high-solidification-rate LPBF process. This leads to the formation of well-bonded interfaces, which can solve the problems of reinforcing particle dispersion and interface bonding with the matrix in conventional manufacturing techniques. Two kinds of diffusional interfaces in composites have been reported. Yan et al[14] indicated that the W and C in WC particles were released and dissolved into the molten pool during LPBF process, and carbides were formed through in-situ reactions with elements from the 18Ni300 matrix, consequently forming a diffusional layer around the particles and improving the microhardness and wear resistance of the composite. Hu et al[15] investigated the diffusional interface of TiCN/AlSi10Mg composites fabricated by LPBF and found that no interfacial reaction occurred between the matrix and TiCN particles, i. e., only diffusion of Al and Si occurred. This phenomenon also enhanced the bonding strength between TiCN particles and the matrix. However, there have been relatively few reports on particle-reinforced 18Ni300 mold steel so far. Moreover, the relationship among reinforcing particles, microstructure, and mechanical properties remains unclear. It is still necessary to continue research on particle-reinforced 18Ni300 mold steel with more excellent properties and to reveal the internal strengthening mechanisms.

Nb has high hardness, strength, melting point, and good thermal stability. It exhibits good chemical compatibility with Fe alloys and easily forms a good interface with 18Ni300, thereby improving the mechanical properties of the matrix. In this study, Nb powders with both coarse and fine particle sizes were selected and separately mixed with 18Ni300 powder. The Nb/18Ni300 composites were fabricated by LPBF. Subsequently, the formed parts were subjected to an aging treatment to explore the interface stability under high-temperature aging conditions and the potential for multi-scale synergistic strengthening effects. The microstructure and mechanical properties of the composites were studied, especially the bonding interface between Nb particles and the 18Ni300 matrix. This research is expected to provide theoretical guidance and technical support for the fabrication of 18Ni300 mold steel with enhanced tensile and wear properties through the combination of LPBF and heat treatment.

2 Experiment

In this research, the used 18Ni300 mold steel was vacuum-atomized powders with particle sizes of 15 – 53 μm. High-purity, low-oxygen, and high-sphericity Nb powders, which were fabricated by TEKNA RF plasma pulverizing equipment, were selected as reinforcing particles. Considering both the powder flowability during the forming process and the reinforcing effect of the particles, two particle size ranges were adopted: 15 – 53 and 5 – 25 μm. The morphology and distribution of the above powders are shown in Fig.1.

The 18Ni300 powder was mechanically mixed with 3wt% coarse Nb powders and 3wt% fine Nb powders for 8 h, separately. This addition amount was determined through preliminary verification experiment, as it yields the greatest strengthening effect. An HBD-280 LPBF system was used to fabricate composite samples under a high-purity argon atmosphere, with a 316L stainless steel plate serving as the substrate. The optimized processing parameters were set as follows: laser power (P)=300 W, scanning speed (V)=1000 mm/s, hatch spacing (H)=100 μm, and layer thickness (T)= 50 μm. The scanning strategy of interlayer laser scanning with a 67° angle offset was used. After additive manufacturing, three sets of samples underwent aging treatment at 490 ℃ for 6 h, followed by air cooling. The composite samples containing coarse and fine Nb powders were named as C-3Nb and F-3Nb, respectively. The as-fabricated samples were denoted as LPBF, and those subjected to aging treatment were denoted as Aging.

To characterize the microstructure and phase distribution at the bonding interface, the longitudinal section (parallel to the building direction) of each sample was polished to a mirror

finish and then etched in a solution consisting of 5vol% HNO_3 and 95vol% ethyl alcohol. The microstructures of the samples were initially observed using an optical microscope (OM, DMI-3000M). For further observation and component analysis, a field emission scanning electron microscope (SEM, Gemini SEM 300) equipped with an energy dispersive spectrometer (EDS, Ultim Max) was subsequently used.

Phase composition of the samples was tested by X-ray diffractometer (XRD, Smart-Lab) using Cu Kα radiation. The hardness of the polished samples was measured by a Rockwell hardness tester (HRS-150) under a load of 1470 N and a dwell time of 10 s. Room-temperature tensile tests were conducted on an electronic universal testing machine (LD24.304) at a crosshead separation rate of 2 mm/min. Friction and wear tests were performed by a universal mechanical tester (UMT-3) under the following conditions: a constant load of 20 N, a loading time of 30 min, a rotational speed of 300 r/min, and an annular wear track with a radius of 3 mm. The friction ball of Si_3N_4 was chosen as the friction pair and all tests were performed at room temperature. The 2D profiles of cross-sectional wear track were scanned using a step profiler (Dektak-XT), and volume wear rates were then calculated using Eq.(1):

$$W_r = \frac{2\pi rA}{FL} \quad (1)$$

where W_r is the wear rate ($mm^3 \cdot (N \cdot m)^{-1}$), r is the radius of the wear track (mm), A is the area of the wear surface (mm^2), F is the load used in the tests (N), and L is the sliding distance (m). After all these tests, SEM was used again to observe the tensile fractographs and wear surfaces.

3 Results and Discussion

Fig. 2 shows the overall morphologies of samples with different Nb addition contents before and after heat treatment. It is observed that there are no obvious inclusions or fusion defects in the LPBF samples. There are obvious layered molten pools in the 18Ni300-LPBF sample due to the strategy of layer-by-layer melting and deposition of the powder bed fusion process (Fig. 2a). Some coarse unmelted Nb particles can be seen in the C-3Nb-LPBF sample (Fig. 2b); their existence disrupts the layered molten pools, leading to irregularities. Some fine unmelted Nb particles are also found in the F-3Nb-LPBF sample (Fig. 2c). Compared with the coarse particles in the C-3Nb-LPBF sample, these fine particles have less impact on the molten pool morphology and are more uniformly distributed in the sample. As shown in Fig. 2d–2f, after heat treatment, the boundaries of the molten pool becomes indistinct. Nevertheless, unmelted Nb particles remain observable in both the C-3Nb-Aging and F-3Nb-Aging samples.

To better characterize the unmelted Nb particles, SEM analysis was performed on the samples. Fig. 3 reveals that the spherical Nb particles are partially melted and uniformly distributed in the composite, which is caused by rapid solidification and strong Marangoni effects in the LPBF process[16–18]. Using ImageJ for quantitative analysis and statistical calculation, the proportions of unmelted particles in the C-3Nb-LPBF, F-3Nb-LPBF, C-3Nb-Aging, and F-3Nb-Aging samples were determined to be 0.97%, 0.52%, 1.48%, and 0.48%, respectively. Furthermore, the particles maintain their original spherical shape, with distinct bonding interfaces of a certain thickness formed between the particles and the matrix (Fig. 3h, 3i, 3k, and 3l). Compared with that of coarse Nb particles, the interface of the fine Nb particles is relatively thinner. After heat treatment, the bonding interfaces of both types of particles further decrease in thickness. These results indicate that, under the same addition amount, when the laser

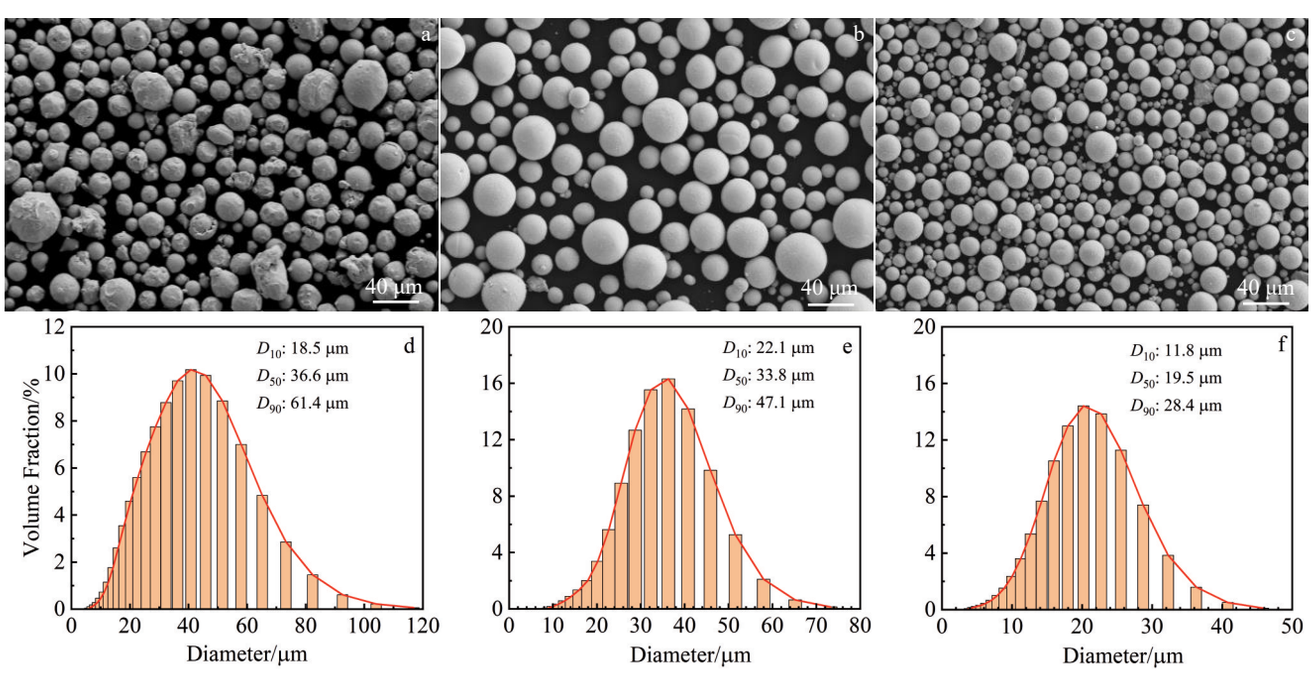

Fig.1 Morphologies (a–c) and particle size distributions (d–f) of different powders: (a, d) 18Ni300, (b, e) coarse Nb, and (c, f) fine Nb

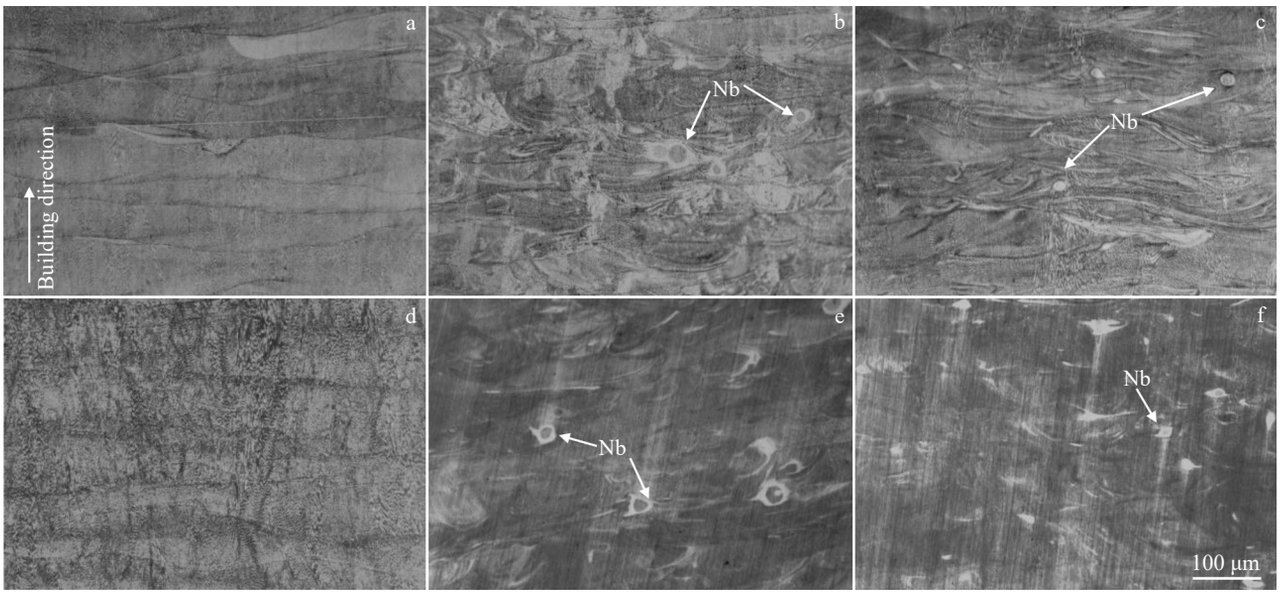

Fig.2 OM images of longitudinal sections of different samples: (a) 18Ni300-LPBF, (b) C-3Nb-LPBF, (c) F-3Nb-LPBF, (d) 18Ni300-Aging, (e) C-3Nb-Aging, and (f) F-3Nb-Aging

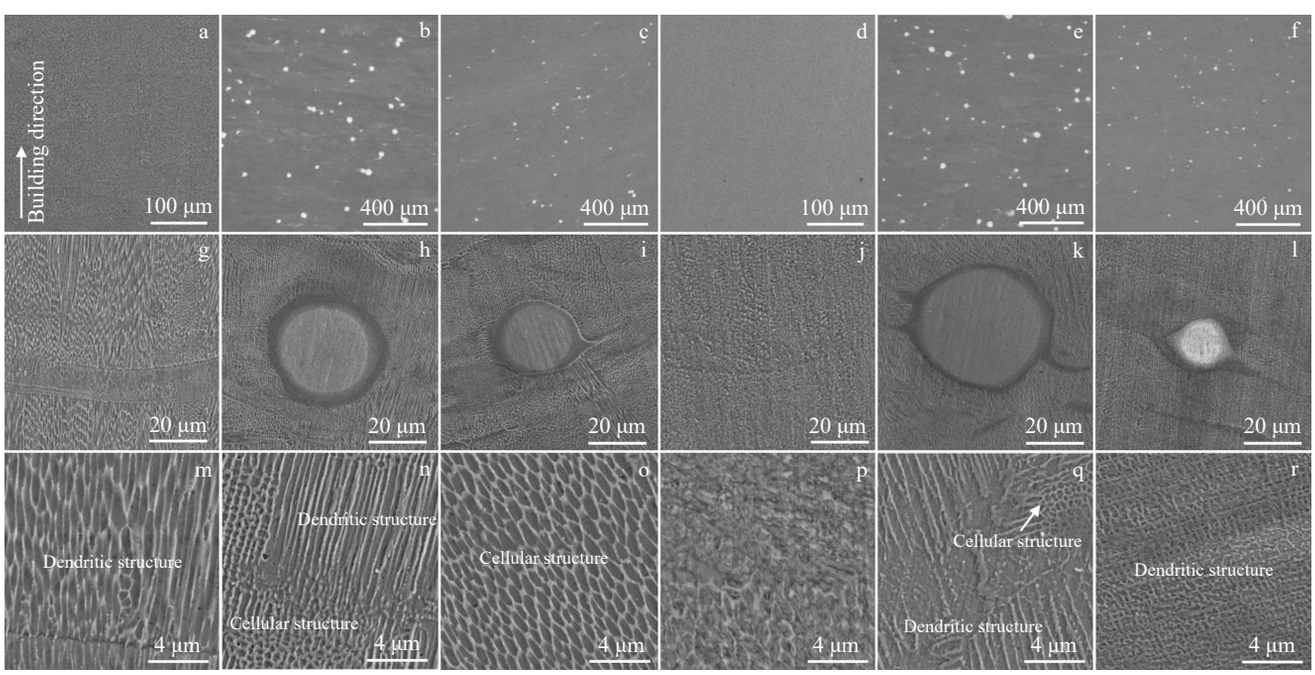

Fig.3 SEM images of longitudinal sections of different samples: (a, g, m) 18Ni300-LPBF, (b, h, n) C-3Nb-LPBF, (c, i, o) F-3Nb-LPBF, (d, j, p) 18Ni300-Aging, (e, k, q) C-3Nb-Aging, and (f, l, r) F-3Nb-Aging

acts on the particle surface, the larger specific surface area of fine Nb particles enables more efficient absorption of laser energy, resulting in more sufficient particle melting. The melted particles rapidly diffuse to form a relatively thin bonding interface. It can be observed that the relatively coarse dendritic structure in 18Ni300-LPBF sample undergoes significant transformation after the addition of Nb particles (Fig. 3m). The microstructure of the C-3Nb-LPBF sample mainly consists of dendritic and cellular structures (Fig. 3n), while the F-3Nb-LPBF sample mainly consists of finer cellular structures (Fig.3o). The size of grains around fine Nb particles (approximately 0.63 μm) is significantly smaller than that around coarse Nb particles (approximately 0.92 μm), indicating that finer Nb particles exert a more obvious grain refinement effect. This difference is determined by the degree of supercooling, which is related to the temperature gradient (G) and the solidification rate (R)[19]. Under a high degree of supercooling, fine grains usually appear due to factors such as high nucleation rate and high growth rate. Due to their larger specific surface area, fine Nb particles absorb more heat,

leading to a larger $G \times R$ value and thus smaller grain sizes. Some grain boundary rupture is observed in the samples after aging treatment, which is consistent with Ref. [20]. During aging, the formation and precipitation of precipitated phases pin the grain boundaries, inhibiting grain growth and resulting in grain refinement (Fig.3q–3r).

An in-depth EDS analysis was performed on the F-3Nb-Aging sample to determine the changes in element content at the interface. As shown in Fig. 4a, distinct color contrasts are presented among the Nb particles, diffusion layer, and 18Ni300 matrix, where the gray area between the particle and matrix corresponds to the diffusion layer. The red arrow denotes the line-scan path used for EDS analysis to investigate the bonding interface. Fig. 4b – 4f show the element distributions across the particle, matrix, and bonding interface. It can be found that the elemental diffusion occurs between the Nb particles and 18Ni300 matrix, and the thickness of the diffusion layer is approximately 3 μm. Elements Fe, Nb, Co, and Ni exhibit a gradient distribution in the interface layer: atoms Fe, Co, and Ni from the matrix diffuse toward the Nb particle interface, while Nb atoms from the particles diffuse outward into the matrix. There is no significant difference in the content of the element Ti because of its low concentration. Fig. 4g further demonstrates that element diffusion occurs at the interface. Along the line-scan path, the Nb content gradually decreases, while the contents of Fe, Ni, and Co gradually increase. These changes in element content indicate that the high thermal energy input from the laser beam during the LPBF process provides the necessary activation energy for elemental diffusion[21]. Such interdiffusion between Nb particles and the matrix contributes to the formation of a strong metallurgical bond and a fully dense interface.

XRD patterns (Fig.5) of 18Ni300 and its composites in both as-built (LPBF) and aged states indicate that the 18Ni300-LPBF sample mainly consists of martensite (α-Fe), with only a small fraction of retained austenite (γ-Fe). With the addition of Nb particles, the intensity of the austenite diffraction peak increases, indicating that Nb particles promote the transformation from martensite to austenite. After aging treatment, the intensity of the austenite peak is further enhanced, which can be attributed to the formation of additional reverted austenite[22–23]. The Nb phase is found in the composite samples, possibly resulting from the further dissolution of Nb particles into the matrix during the aging treatment.

As depicted in Fig. 6a, the Rockwell hardness of the Nb/18Ni300 composites increases with the addition of Nb particles, and the F-3Nb-LPBF sample has the highest hardness, rising from 36.9 HRC (base alloy) to 42.6 HRC. This is mainly due to solution strengthening and fine grain strengthening mechanisms[24–26]. On the one hand, atoms released by Nb particles during melting dissolve into the matrix, where they interact with dislocations to inhibit their movement, thereby increasing hardness. On the other hand, the addition of fine Nb particles refines the composite grains, resulting in more grain boundaries that act as obstacles to dislocation movement. After aging treatment, the hardness of all samples further increases: the hardness of F-3Nb-Aging sample reaches 56.1 HRC. This is the result of the combined effects of further grain refinement and the dispersion of precipitates, both of which effectively hinder dislocation movement.

The addition of Nb particles improves the hardness of Nb/18Ni300 composites, and high hardness usually has a positive impact on wear resistance. Therefore, wear tests were conducted on the samples to evaluate the wear resistance.

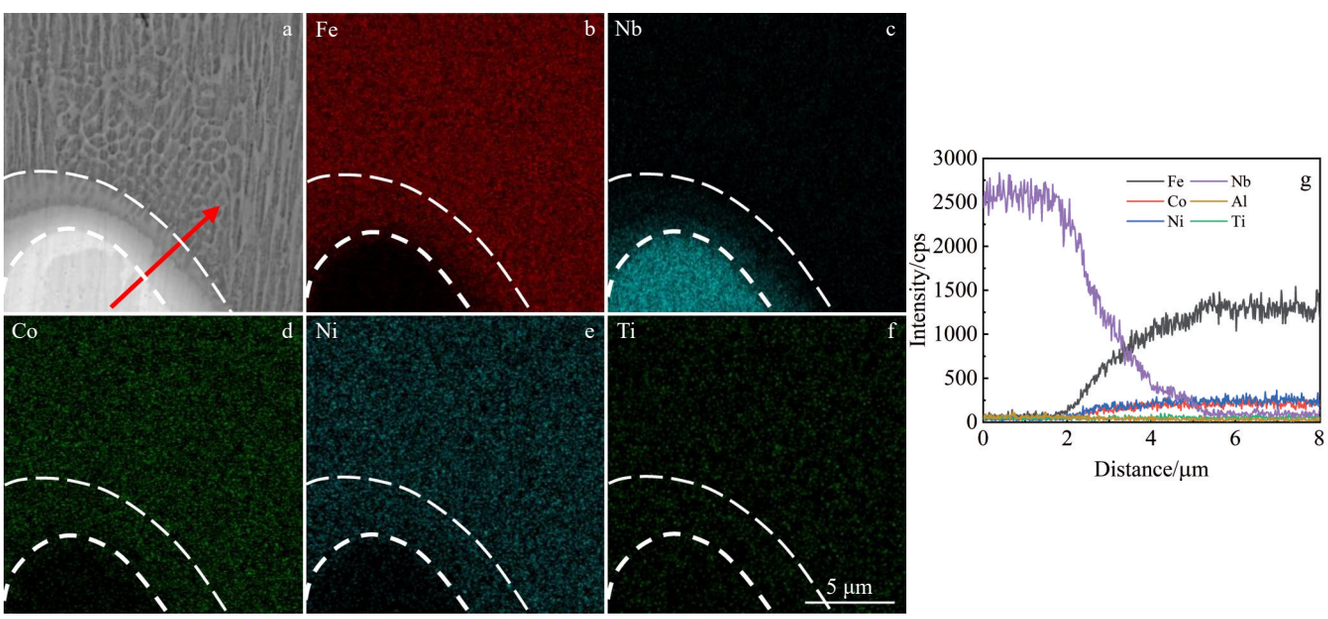

Fig.4 SEM image (a), corresponding EDS elemental mappings (b–f), and EDS line-scan results along red arrow in Fig. 4a (g) of F-3Nb-Aging sample

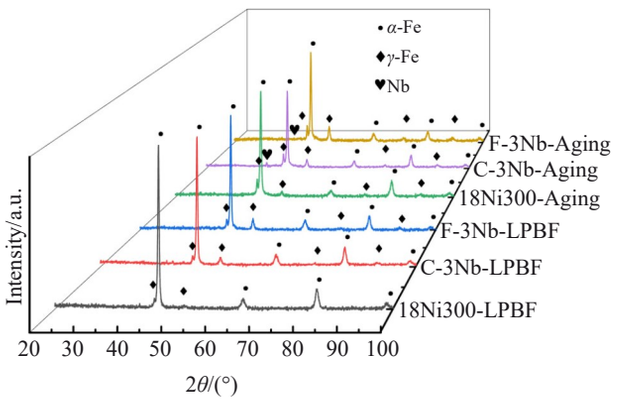

Fig.5 XRD patterns of different samples

Fig. 6b – 6c depict the friction curves of the samples. The average coefficient of friction (COF) of the 18Ni300-LPBF, C-3Nb-LPBF, F-3Nb-LPBF, 18Ni300-Aging, C-3Nb-Aging, and F-3Nb-Aging samples is 0.63, 0.41, 0.44, 0.58, 0.39, and 0.53, respectively. It can be observed from Fig. 6b that the COF of the 18Ni300-LPBF sample has a large fluctuation at the beginning and then tends to stabilize. This behavior may be explained by the uneven surface at the start of friction, which causes a rapid increase in frictional force between the 18Ni300 base alloy and the friction pair, resulting in a sharp rise in COF. As wear progresses, the actual contact area increases, and the surface becomes relatively flat, leading to a decrease in local stress and COF. This stage is known as the running-in period[27]. As wear intensifies, generated debris may act as abrasive particles between the contact surfaces, causing the COF to rise again. When the surface layer changes reach a certain level, the COF enters a stable state. In contrast, the composites have smaller fluctuations at the beginning, and their overall COF is significantly lower than that of the 18Ni300 base alloy. This is because the dispersed hard Nb particles in the composites can bear part of the load during friction. The COF of the C-3Nb-LPBF sample is slightly lower than that of the F-3Nb-LPBF sample, possibly because of the better load-bearing capacity of coarse Nb particles. Fig.6c shows that the aging treatment reduces the COF of the 18Ni300 base alloy and its composites, and the C-3Nb-Aging sample exhibits the lowest COF. The 18Ni300-Aging sample follows the same wear mechanism as that of 18Ni300-LPBF sample. The difference is that its initial COF peak is relatively low, which may be attributed to the strengthening effect of the precipitated phases. It should be noted that, the COF of the composites generally shows a slow upward trend over time, which may be ascribed to the continuous exfoliation of Nb particle debris into the interface between the sliding surfaces[28].

The volume wear rates after the wear test are presented in Fig. 7a. The volume wear rate of 18Ni300-LPBF sample is 19.7×10^{-6} mm^3/(N·m), whereas that of the C-3Nb-LPBF and F-3Nb-LPBF samples are 3.5×10^{-6} and 4.4×10^{-6} mm^3/(N·m), respectively. It can be found that the addition of Nb particles significantly reduces the volume wear rates of the composites, especially the addition of coarse particles. After aging treatment, the volume wear rate of the C-3Nb-Aging sample further decreases to 1.7×10^{-6} mm^3/(N·m), which is 90% lower than that of the 18Ni300-Aging sample. Fig.7b–7c display the 2D cross-sectional profiles of the wear tracks. As shown in Fig. 7b, the 18Ni300 base alloy exhibits wide and deep wear pits, indicating severe wear. Due to the load-bearing effect of unmelted Nb particles in the matrix, the composites demonstrate better wear resistance. The width of wear pits of the C-3Nb-LPBF and F-3Nb-LPBF samples is approximately half of that of the base alloy, and the former has shallower wear pits. In addition, the morphologies of the wear pits of the aged samples show no significant changes (Fig.7c), except for the C-3Nb-Aging sample, whose pits become shallower. The above analysis is consistent with the COF results. Fig. 7d–7o display SEM images of the worn surfaces. For the 18Ni300-LPBF sample, rows of ploughing grooves parallel to the sliding direction and a small amount of spalled debris can be clearly observed (Fig.7d and 7j), indicating that abrasive wear and minor adhesive wear occur. On the worn surfaces of the composites, delamination phenomena are observed (Fig. 7k and 7l). The lamellae contain micro-cracks and are partially sheared. This is because the material transfer between contact surfaces during wear generates tensile stress, causing micro-cracks and even spalling on the surface. The worn surfaces are relatively smooth, with only shallow ploughing grooves, indicating that the wear mechanisms are adhesive wear and abrasive wear. After aging treatment, only the worn surface of the C-3Nb-Aging sample has significant changes: numerous

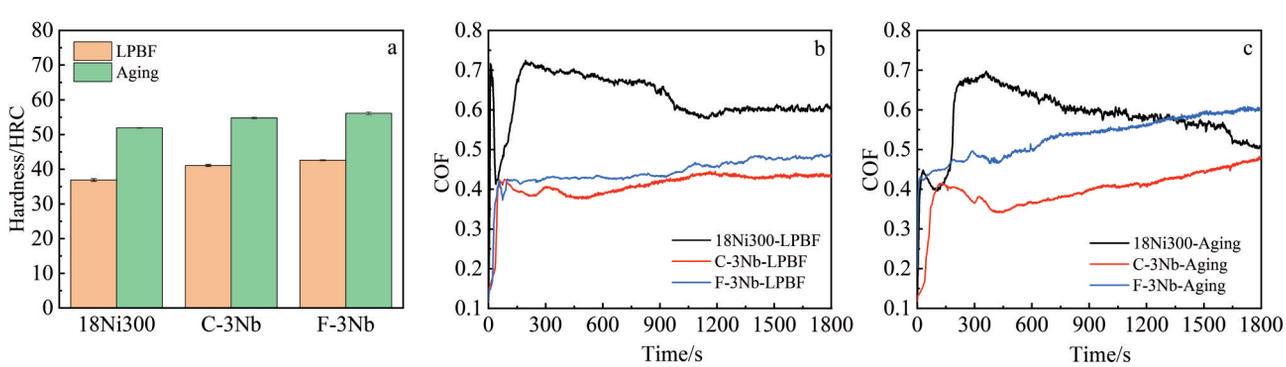

Fig.6 Hardness of different samples (a); COF curves of different samples under LPBF state (b) and aged state (c)

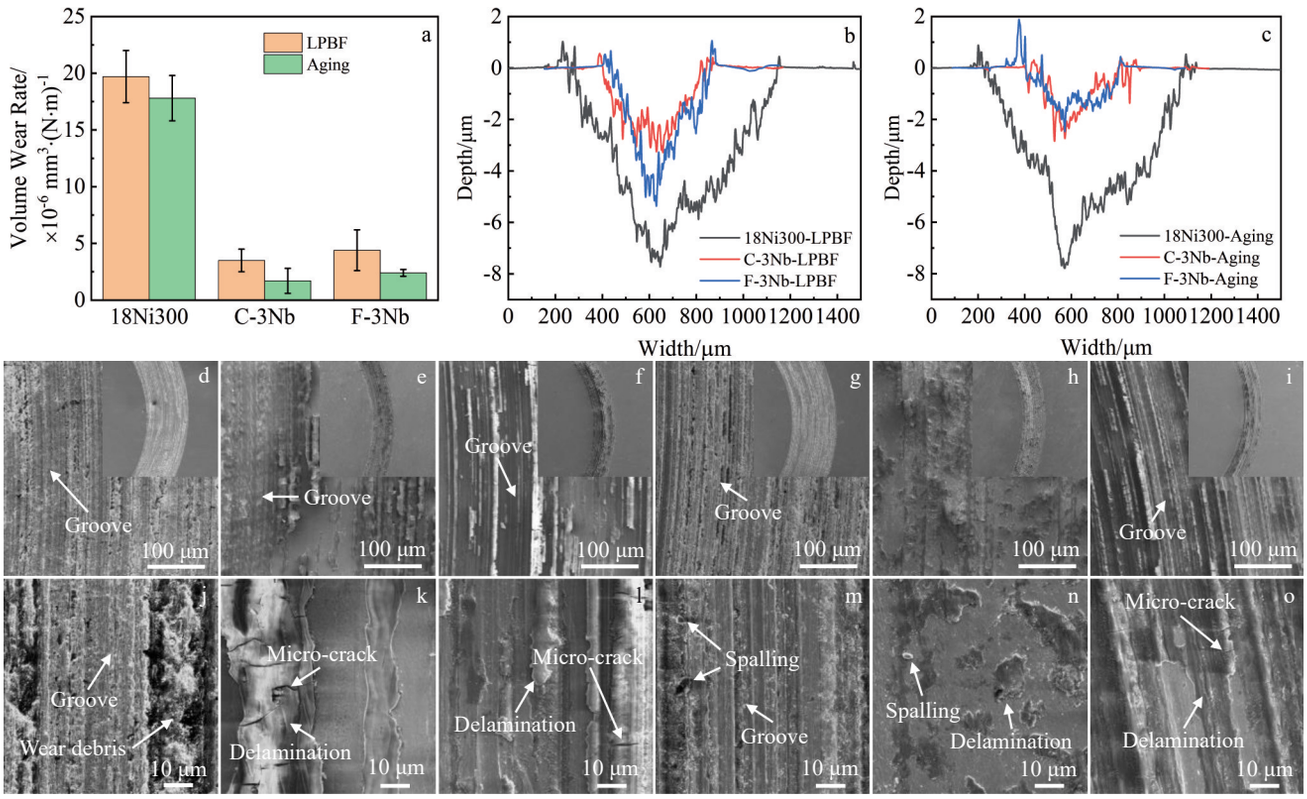

Fig.7 Volume wear rates of different samples (a); 2D cross-sectional profiles of wear tracks of samples under LPBF state (b) and aged state (c); SEM images of worn surfaces of 18Ni300-LPBF (d, j), C-3Nb-LPBF (e, k), F-3Nb-LPBF (f, l), 18Ni300-Aging (g, m), C-3Nb-Aging (h, n), and F-3Nb-Aging (i, o) samples

spalls and wear debris can be found, along with large flaky delaminations adhering to the surface. The worn surface becomes smoother without visible ploughing grooves (Fig. 7h and 7n), indicating further enhanced wear resistance. From the above results, it can be concluded that the addition of Nb particles significantly improves the wear resistance of the Nb/18Ni300 composites, and coarse Nb particles have a better load-bearing capacity. Aging treatment has a relatively limited effect on the overall wear resistance improvement, exerting a greater impact only on the sample containing coarse Nb particles.

Fig. 8a – 8b show the engineering stress-engineering strain curves and tensile properties of 18Ni300 in both LPBF and aged states. It can be seen that the ultimate tensile strength, yield strength, and elongation at break of the Nb/18Ni300 composite are slightly decreased after adding Nb particles. The C-3Nb-LPBF sample exhibits the poorest tensile property: its ultimate tensile strength decreases from 1264 MPa (base alloy) to 1210 MPa, and its elongation at break drops from 15% to 4%. After aging treatment, all three samples show an increase in ultimate tensile strength and a decrease in elongation at break. The F-3Nb-Aging sample has the highest ultimate tensile strength (1892 MPa) and yield strength (1842 MPa), albeit at the cost of elongation at break (3%). Phase transformation, microstructural changes, and the bonding interface are the main factors influencing the above variations in mechanical properties.

The fracture morphologies of the 18Ni300 base alloy and its composites after the tensile testing were obtained to explore the fracture mechanisms (Fig. 8c – 8n). For the 18Ni300-LPBF sample, the fracture surface contains numerous dimples with varying sizes and shows obvious necking (Fig. 8c and 8i), which are typical characteristics of ductile fracture. The presence of tearing ridges further indicates its ductile fracture behavior. Fig. 8d–8e show that the unmelted Nb particles are observed on the fracture surfaces of the Nb/18Ni300 composites. Most of these particles still maintain their original spherical shape, indicating interfacial debonding. The weak interface may act as a crack source during the tensile process, leading to a reduction in the strength of the composites (Fig. 8a). The fracture of the C-3Nb-LPBF sample displays cleavages as well as some dimples (Fig. 8d and 8j), indicating a mixed ductile-brittle fracture mode. For the F-3Nb-LPBF sample, its fracture features include elongated dimples, tearing ridges, and sparse cleavages (Fig. 8e and 8k), suggesting a predominantly ductile fracture mechanism. Fractured unmelted Nb particles are found on the fracture surfaces of the aged composites, indicating the formation of a strong bonding interface around Nb particles. These high-strength and high-hardness particles play a role in preventing crack propagation during the tensile process. Moreover, all aged samples exhibit mixed ductile-

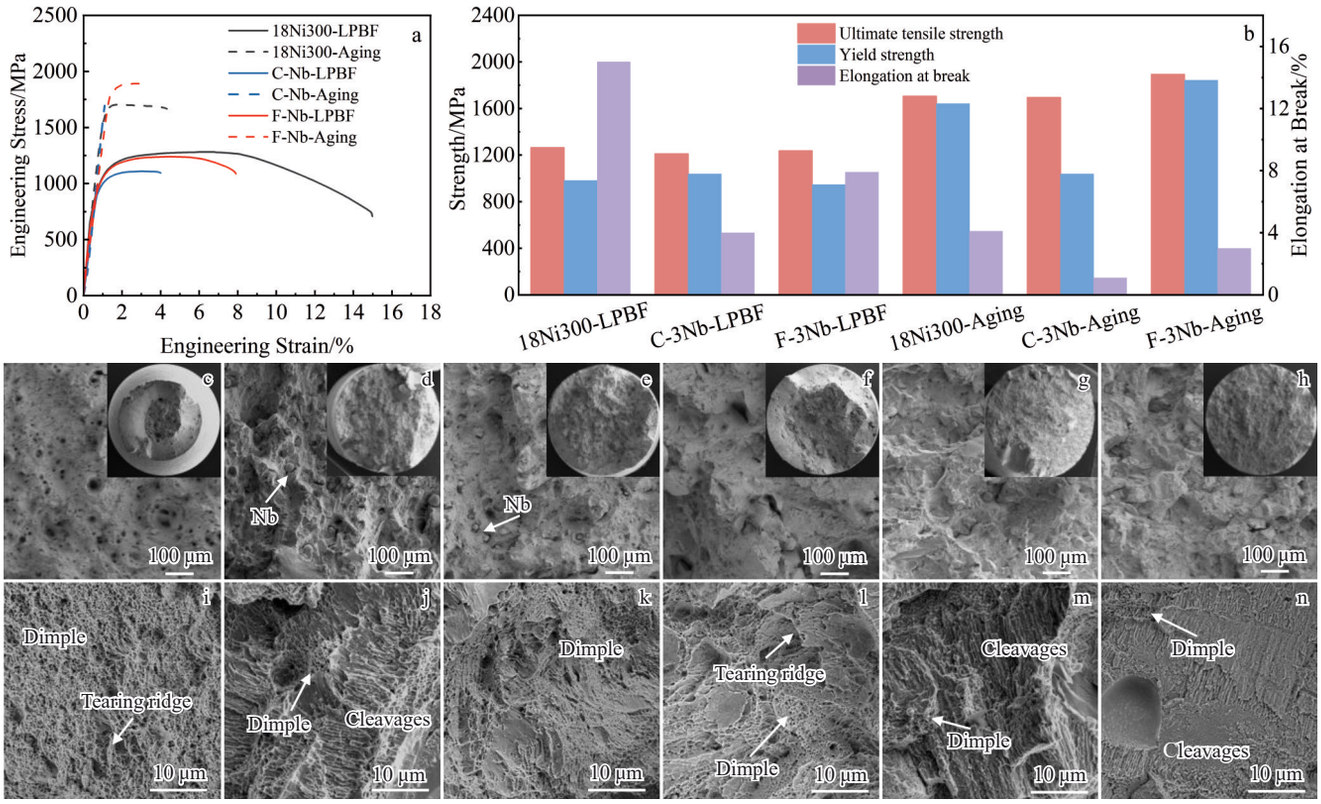

Fig.8 Engineering stress-engineering strain curves (a), tensile properties (b), and SEM images of fracture surfaces (c–n) of different samples: (c, i) 18Ni300-LPBF, (d, j) C-3Nb-LPBF, (e, k) F-3Nb-LPBF, (f, l) 18Ni300-Aging, (g, m) C-3Nb-Aging, and (h, n) F-3Nb-Aging

brittle fracture features. Among them, C-3Nb-Aging sample shows more cleavages (Fig. 8g and 8m), which is consistent with its elongation at break. The strong bonding interface between Nb particles and the 18Ni300 matrix is the reason for the increased ultimate tensile strength and decreased elongation at break of the composites. As previously mentioned in SEM analysis, fine Nb particles have a thinner bonding interface than coarse Nb particles. Combined with the tensile properties, it can be concluded that the thinner the bonding interface, the higher the strength.

4 Conclusions

1) 18Ni300 composites reinforced by Nb particles of different particle sizes are fabricated by LPBF. It is found that the unmelted Nb particles are evenly distributed in the matrix and can refine the grains, with fine Nb particles demonstrating a more significant refining effect. A bonding interface of a certain thickness forms around the unmelted Nb particles, and the bonding interface of fine Nb particles is relatively thinner. After aging treatment, the grains of the samples become finer and the bonding interface of unmelted Nb particles also becomes thinner. EDS results confirm elemental diffusion between Nb particles and the matrix, contributing to the formation of a strong metallurgical bond and a dense interface.

2) The main phases of 18Ni300 sample are composed of martensite (α-Fe) and a small amount of retained austenite (γ-Fe). The addition of Nb particles promotes the transformation from α-Fe to γ-Fe, and aging treatment further facilitates the formation of reverted austenite.

3) Both the addition of Nb particles and aging treatment improve the Rockwell hardness and wear properties of the samples. Specifically, after heat treatment, the hardness of the sample added with fine Nb particles increases from 36.9 HRC (base alloy) to 56.1 HRC, and the volume wear rate of the sample added with coarse Nb particles decreases from 19.7×10^{-6} mm^3/(N·m) (base alloy) to 1.7×10^{-6} mm^3/(N·m).

4) Adding Nb particles slightly decreases the ultimate tensile strength and elongation at break of the composites. After aging treatment, the sample added with fine Nb particles have the highest ultimate tensile strength (1892 MPa) and yield strength (1842 MPa), albeit with a relatively low elongation at break (3%).

References

1 Vishwakarma J, Chattopadhyay K, Santhi S N C. *Materials Today Communications*[J], 2023, 35: 105825

2 Zhao Z J, Wang L, Kong D C *et al*. *Materials Characterization*[J], 2022, 189: 111938

3 Kang N, Ma W Y, Heraud L *et al*. *Additive Manufacturing*[J], 2018, 22: 104

4 Li Zhenhua, Teng Baoren, Yao Bibo *et al*. *Rare Metal Materials and Engineering*[J], 2023, 52(1): 283 (in Chinese)

5 Han R, Li X P, Chen H R *et al*. *Journal of Materials Research*

and Technology[J], 2023, 24: 4517
6 Tekin T, Ischia G, Naclerio F *et al*. *Materials Science and Engineering A*[J], 2023, 872: 144921
7 Ong J K, Tan Q Y, Silva A *et al*. *Materials Today: Proceedings*[J], 2022, 70: 438
8 Mao Z F, Lu X D, Yang H R *et al*. *Materials Science and Engineering A*[J], 2022, 830: 142334
9 Guo W F, Guo C, Zu Q. *Materials Science Forum*[J], 2018, 941: 22160
10 Wang M H, Yan H, Zhang P L *et al*. *Optics & Laser Technology*[J], 2024, 176: 110918
11 Chen D, Pan Q Q, Liu Z Q *et al*. *Journal of Materials Research and Technology*[J], 2024, 30: 1889
12 Zhang Y M, Yu Y F, Wang L *et al*. *Acta Materialia*[J], 2022, 235: 118086
13 Bhowmik A, Zhai W G, Zhou W *et al*. *Materials Characterization*[J], 2021, 179: 111360
14 Yan X C, Chen C Y, Zhao R X *et al*. *Surface and Coatings Technology*[J], 2019, 371: 355
15 Hu Z J, Zhao Z, Deng X *et al*. *Materials Chemistry and Physics*[J], 2022, 283: 125996
16 Liu Qi, Yang Guang, Yin Jun *et al*. *Rare Metal Materials and Engineering*[J], 2024, 53(7): 2094 (in Chinese)
17 Wang Qiuping, Guan Jieren. *Rare Metal Materials and Engineering*[J], 2024, 53(3): 676 (in Chinese)
18 Ni Haohan, Zeng Qi, Zhang Kai *et al*. *Rare Metal Materials and Engineering*[J], 2023, 52(6): 2302 (in Chinese)
19 Xia Y L, Chen H N, Liang X D *et al*. *Journal of Manufacturing Processes*[J], 2021, 68: 1694
20 Ansell T Y, Ricks J P, Park C *et al*. *Metals*[J], 2020, 10(1): 218
21 Yan X C, Huang C J, Chen C Y *et al*. *Surface and Coatings Technology*[J], 2019, 371: 161
22 Jägle E A, Choi P P, Van Humbeeck J *et al*. *Journal of Materials Research*[J], 2014, 29: 2072
23 Pereloma E V, Shekhter A, Miller M K *et al*. *Acta Materialia*[J], 2004, 52: 5589
24 Li X F, Feng Y H, Liu B *et al*. *Journal of Alloys and Compounds*[J], 2019, 788: 485
25 Zou Y M, Tan C L, Qiu Z G *et al*. *Additive Manufacturing*[J], 2021, 41: 101971
26 Lan C X, Hu Y L, Wang C Z *et al*. *Additive Manufacturing*[J], 2024, 85: 104153
27 Gu D D, Ma J, Chen H Y *et al*. *Composite Structures*[J], 2018, 192: 387
28 Guo X X, Ma M, Zhang S F *et al*. *Tribology International*[J], 2024, 194: 109536

Nb添加对LPBF成形18Ni300模具钢拉伸和磨损性能的影响

简昌煌[1,2]，杨　洋[1]，王成勇[1]，余博文[1,2]，牛留辉[2]，胡高峰[2]，刘建业[2]，黄正华[2]
(1. 广东工业大学 机电工程学院 高性能工具全国重点实验室，广东 广州 510006)
(2. 广东汉邦激光科技有限公司 广东省金属3D打印工程技术研究中心，广东 中山 528427)

摘　要：激光粉末床熔融（LPBF）技术凭借其制造复杂形状的卓越能力和调控微观结构的出色性能，在制备18Ni300模具钢方面极具优势，并且在注塑、压铸以及冲压模具等领域有着广泛应用。在模具钢中添加增强颗粒是提升其性能的有效手段。采用2种不同粒径的Nb粉末，利用LPBF技术制备了Nb/18Ni300复合材料，并对其微观结构和力学性能展开研究。结果显示，未熔Nb颗粒在基体中均匀分布且细化了基体晶粒，尤其是细粒径的Nb颗粒。此外，颗粒与基体间发生了元素扩散。18Ni300基体的主相为α-Fe和少量γ-Fe。添加Nb后，部分α-Fe转变为γ-Fe，并出现未熔Nb相。Nb的加入还提高了复合材料的硬度和耐磨性能，但略微降低了其拉伸性能。时效处理后，熔池和晶界变得模糊，晶粒进一步细化，颗粒周围的界面变薄。时效处理还促进了逆转奥氏体的形成。基础合金的硬度、极限抗拉伸强度以及体积磨损率分别达到51.9 HRC、1704 MPa和17.8×10^{-6} mm^3/(N·m)；相比之下，添加了细Nb颗粒的样品具有最大的硬度（56.1 HRC）、极限抗拉伸强度（1892 MPa）和屈服强度（1842 MPa），添加粗Nb颗粒样品的体积磨损率降低了90%，降至1.7×10^{-6} mm^3/(N·m)。

关键词：激光粉末床熔融；18Ni300模具钢；Nb添加；微观组织；力学性能

作者简介：简昌煌，男，1999年生，硕士生，广东工业大学机电工程学院高性能工具全国重点实验室，广东 广州 510006，E-mail：931849898@qq.com